

https://dspace.org/

Stagnation heat transfer on a concave surface cooled by unconfined slot jet

Aziz, Maurel Nguepnang

2015

https://hdl.handle.net/10539/31662

Aziz, Maurel Nguepnang. 2015. Stagnation heat transfer on a concave surface cooled by unconfined slot jet. University of the Witwatersrand, https://hdl.handle.net/10539/31662

Downloaded from a DSpace repository. https://dspace.org/

STAGNATION HEAT TRANSFER
ON
A CONCAVE SURFACE COOLED
BY
UNCONFINED SLOT JET

Maurel Nguepnang Aziz

A dissertation submitted to the faculty of Engineering and the Built Environment, University of the Witwatersrand, Johannesburg, in fulfilment of the requirements for the degree of Master of Science in Engineering.

Johannesburg, 2015

DECLARATION

I declare that this dissertation is my own unaided work. It is being submitted to the degree of Master of Science to the University of the Witwatersrand, Johannesburg. It has not been submitted before any degree or examination to any other university.

……...
(Signature of Candidate)

……day of ……year……

ABSTRACT

Heat transfer at the stagnation point on a concave surface and on a flat plate subjected to unconfined slot jet impingement is characterized and compared at a fixed jet Reynolds number of Re_B = 20000. The concave surface diameter-to-slot width ratio is fixed at 9.0 whilst the slot exit-to-target surface distance, *H/B*, varies from 0.5 to 20.0. In particular, the non-monotonic variation of heat transfer at the stagnation point with *H/B* is fluidically explained. The present results clarify that the deflection zone formed on the target surface as a result of the jet impingement leads to the upstream shift of the peak in turbulence strength that exactly coincides with the peak of heat transfer at the stagnation point. With the concave surface, the impinging jet deflected radially on the surface is re-entrained into the incoming jet due to the curvature, which causes the shortening of the potential core of the slot jet and the longitudinal upstream shift of the peak in turbulence strength compared to the flat plate. Therefore, the peak in heat transfer at the stagnation point occurs at shorter *H/B* on the concave surface than on the flat plate.

ACKNOWLEDGMENTS

First and foremost I would like to thank my supervisor Professor Kim for his supervision and assistance throughout this journey, this work would not have been possible without his immeasurable help. Secondly, I want to thank my mother for the financial and emotional support she provided me with. Lastly, but not least I want to show my appreciation to all the member of the Thermo-fluid Lab., which all in some degree assisted me during the completion of this work.

CONTENTS

DECLARATION		2
ABSTRACT		3
ACKNOWLEDGEMENTS		4
LIST OF FIGURES		6
LIST OF TABLES		8
LIST OF SYMBOLS		9
1.	INTRODUCTION	11
	1.1. Background	11
	1.2. Objectives	13
2.	EXPERIMENTAL DETAILS	14
	2.1. Test rig	14
	2.2. Pressure and velocity measurements	14
	2.3. Turbulence measurement	15
	2.4. Flow visualization using helium bubbles	16
	2.5. Heat transfer measurement	16
	2.6. Heat transfer mapping using an infrared (IR) thermography	17
3.	FREE SLOT JET CHARACTERISTICS	22
4.	HEAT TRANSFER AT THE STAGNATION POINT ON A FLAT PLATE	24
	4.1. Heat transfer at the stagnation point	24
	4.2. Centerline flow properties	25
	4.3. Summary	27
5.	HEAT TRANSFER AT THE STAGNATION POINT ON A CONCAVE SURFACE	28
	5.1. Heat Transfer at the Stagnation Point	29
	5.2. Centerline velocity	30
	5.3. Centerline turbulence strength	32
	5.4. Flow acceleration near the stagnation point	33
6.	SUMMARY	34
7.	CONCLUSIONS	35
8.	REFERENCES	36

LIST OF FIGURES

1. Internal cooling schemes adopted in a high pressure gas turbine blade design, showing jet impingement on a concave surface at the leading edge 12
2. Heat transfer at the stagnation point, Nu_{stag} varied with a jet-to-target surface distance H normalized by a characteristic length, H/B or H/Dj where B is the slot width and Dj is the round jet diameter 13
3. Schematic of the slot jet impingement on a flat plate or a concave surface (D/B = 9.0) 14
4. Schematic of infrared temperature measurement on a flat plate and concave surface. 17
5. View angle effect on IR temperature normalized by thermocouple temperature (T_{IR}/T_{TC}) on a flat plate versus (a) the IR camera view angle α, (b) the radial location s 21
6. View angle effect on IR temperature normalized by thermocouple temperature (T_{IR}/T_{TC}) on a flat plate versus (a) the IR camera view angle α, (b) the radial location s 22
7. Variation of (a) Centerline velocity (w_0) and (b) Turbulence intensity (w_{rms}/w_0) and strength (w_{rms}/w_e), along the jet axis at Re_B = 20000 24
8. Heat transfer at the stagnation point Nu_B varying with the jet exit-to-flat plate distance H/B at Re_B = 20000 25
9. Variation of normalized centerline velocity along the jet axis with impingement on a flat plate at Re_B = 20000 25
10. Turbulence strength (w_{rms}/w_e): (a) along the jet centerline axis (i.e., the z-axis); (b) at 0.5B upstream from a flat plate 26
11. Local heat transfer along the flat plate and concave surface (D/B = 9.0), (a) H/B = 4.0, (b) H/B = 6.0, (c) H/B = 12.0. 28
12. Heat transfer at the stagnation point of a concave surface cooled by a slot jet at Re_B = 20000 where the data for a flat plate under the same conditions are included for comparison 30
13. Variation of normalized centerline velocity along the jet axis (i.e., the z-axis) of a slot jet impinging on a concave surface at Re_B = 20000 31

14. Streaklines of the slot jet impinging: (a) on a flat plate; (b and c) on a concave surface (D/B = 9.0), for Re_B = 20000 31

15. Turbulence strength (w_{rms}/w_e): (a) along the jet axis (i.e., the z-axis); (b) at 0.5B upstream of a concave surface 33

16. Flow acceleration: (a) lateral pressure distribution on the flat and concave surface; and lateral velocity normalized by the jet exit velocity v_s/w_e along the target surfaces, (b) at H/B = 4.0, (c) at H/B = 12.0 34

LIST OF TABLES

Table 1. List of impingement cooling studies on a flat plate and concave surface where (a) jet exit-to-target surface distance (H/B or H/D_j); (b) length of potential core of the free jet (z/B or z/D_j); (c) location of peak in heat transfer at the stagnation point (H/B or H/D_j); (d) location of peak in turbulence strength (in free exit, z/B or z/D_j) 40

Table 2. Test parameters and conditions 43

Table 3. Infrared camera settings 43

Table 4. Infrared calibration fourth order polynomial. 43

LIST OF SYMBOLS

Slot width along the y-axis, m	B
Pressure coefficient (Eq. (2))	C_p
Concave surface diameter, m	D
Round jet diameter, m	D_j
Slot jet exit-to-target surface distance, m	H
Convective heat transfer coefficient at the stagnation point, W/(m^{2}K)	h_s
Thermal conductivity, W/(mK)	k
Nusselt number at the stagnation point based on the slot width (Eq. (4))	Nu_B
Static pressure on the target surface, Pa	p
Static pressure at the slot jet exit, Pa	p_e
Total (stagnation) pressure at *S/B* equal to 0, Pa	p_t
Conduction heat loss, W/m^2	q''_{cond}
Net heat flux removed from the target surface by the slot jet, W/m^2	q''_{net}
Total heat flux, W/m^2	q''_t
Radiation heat loss, W/m^2	q''_{rad}
Jet Reynolds number based on the slot width (Eq. (1))	Re_B
Coordinate along the flat and concave surfaces	S
Ambient air temperature, K	T_a
Thermocouple measured temperature on the target surface, K	T_{IR}
Jet temperature measured at the jet exit, K	T_e
Jet temperature along the z-axis, K	T_0
Surface temperature on the flat/concave surfaces, K	T_s
Thermocouple measured temperature on the target surface, K	T_{TC}
Lateral velocity component of the jet leaving the stagnation point, m/s	v_s
Axial velocity component of the jet discharged from the slot, m/s	w
Jet exit velocity at y and z equal to 0, m/s	w_e
Axial centerline velocity at y equal to 0, m/s	w_0
Root mean square of the velocity fluctuation (Eq. (3)), m/s	w_{rms}
Instantaneous velocity fluctuation, m/s	w'_i
Coordinate along the slot length	x
Coordinate along the slot width	y

Axial coordinate coinciding with the jet centerline axis	z

Greek Symbols

Density of air, kg/m^3	ρ
Viscosity of air, kg/(ms)	μ

Subscripts

Index of summation	i
Root mean square	rms

1. INTRODUCTION

1.1. Background

Jet impingement cooling/heating provides high rate of heat transfer compared to other single-phase heat transfer schemes, which has led to numerous engineering applications requiring high heat removal capacity [1-4]. Analysis of impinging jet heat transfer is complex and involves many parameters including (a) jet Reynolds number, (b) jet-to-flat plate distance, (c) jet nozzle shape (two-dimensional (slot) jet or three-dimensional (round) jet), (d) jet arrangement e.g., single or multiple arrays, (e) target surface geometry (flat plate, concave surface and convex surface e.g., circular cylinder), and (f) turbulence within the jet.

A multitude of previous studies have documented that the overall and local impinging jet heat transfer characteristics on a flat plate (as the most simplistic configuration in all impinging jet configurations) depend strongly on the jet-to-flat plate distance, H, among other parameters [5-16]. Depending on the longitudinal position relative to the length of potential core of the jet, either two peaks of local heat transfer (a primary peak at the stagnation point and a second peak off from the stagnation point) or a single peak (only at the stagnation point). The appearance and disappearance of the second peak are associated with the laminar to turbulent transition in the boundary layer of the wall jet formed on the flat plate as a result of the lateral deflection of the jet.

Local heat transfer, especially at the stagnation point where the highest heat transfer and pressures exist on a target surface (e.g., flat plate) due to stagnation, substantially varies with the jet-to-flat plate distance H. It has been observed that the highest heat transfer at the stagnation point occurs at very small jet-to-flat plate distances due to the local acceleration of the fluid between the jet nozzle and the flat plate and a significant increase in local turbulence level [12-14, 17]. As the jet-to-flat plate distance is further increased, heat transfer at the stagnation point non-monotonically varies [12-14, 18, 19] experiencing: (a) a gradual decrease, (b) to a local minimum, (c) a gradual increase, (d) to a local maximum (peak), and (e) a monotonic decrease.

Gardon and Akfirat [5] who experimentally investigated the effect of turbulence on the variation of heat transfer at the stagnation point on a flat plate subjected to turbulent slot jet impingement, attributed the non-monotonic variation to the competition between the centreline turbulence level and the arrival velocity of the jet. Based primarily on the observed free jet characteristics, they conjectured that; (i) inside the potential core of the slot jet, the

increase in turbulence level while the centerline velocity remains constant, causes the increase and peak of heat transfer at the stagnation point; (ii) outside the potential core of the slot jet, the diminishing centerline velocity dominates over the turbulence level, consequently decreasing heat transfer at the stagnation point. All subsequent works [5-16, 18-22] have referred to this argument as the fluidic mechanisms of the observed non-monotonic variation of heat transfer at the stagnation point.

In high heat flux applications such as internal cooling of gas turbine blades, jet impingement at the leading edge of the blades is on a concave surface (Fig. 1). It has been reported that the variations of local heat transfer including at the stagnation point are similar to those observable on a flat plate [18-22]. Results and interpretations of selected previous studies on impinging jet heat transfer at the stagnation point on a flat plate and a concave surface subjected to turbulent jets at the similar jet Reynolds number range (Re_j ~ 20000) with detailed parameters are collated in Table 1 and plotted in Fig. 2. The data consistently shows the above-mentioned non-monotonic variation of heat transfer at the stagnation point of a target surface (both a flat plate and a concave surface). Detailed longitudinal location (H/B or H/D_j) corresponding to each heat transfer feature differs, depending on individual jet characteristics such as the length of potential core.

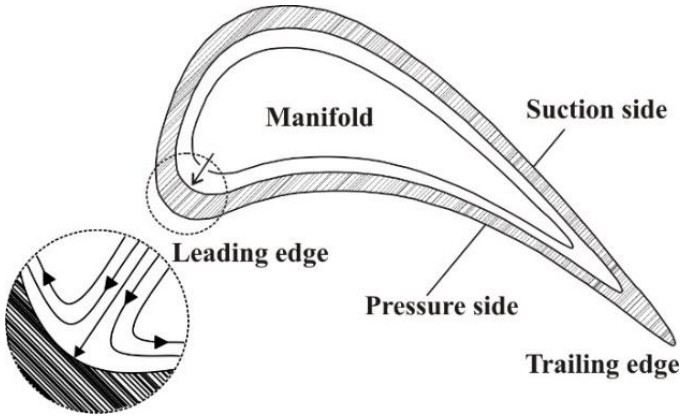

Figure 1. Internal cooling schemes adopted in a high pressure gas turbine blade design, showing jet impingement on a concave surface at the leading edge.

The variation of heat transfer at the stagnation point with the jet-to-flat plate distance has been conjectured [5] and widely accepted [16, 18-22] to depend on the fluidic characteristics of the jet in free exit. However, with the presence of a target surface, the fluidic characteristics of the jet are altered due to the impingement [18, 23-26]. The jet approaching the target surface is decelerated and eventually stagnated, forming a “deflection

zone." Therefore, the flow characteristics of the free jet may not constitute an accurate representation of the impinging jet features, which requires clarification. In addition, especially with a concave surface, it is not clear whether the longitudinal variation of heat transfer at the stagnation point with the impinging distance is caused by the same fluidic mechanisms as with a flat plate.

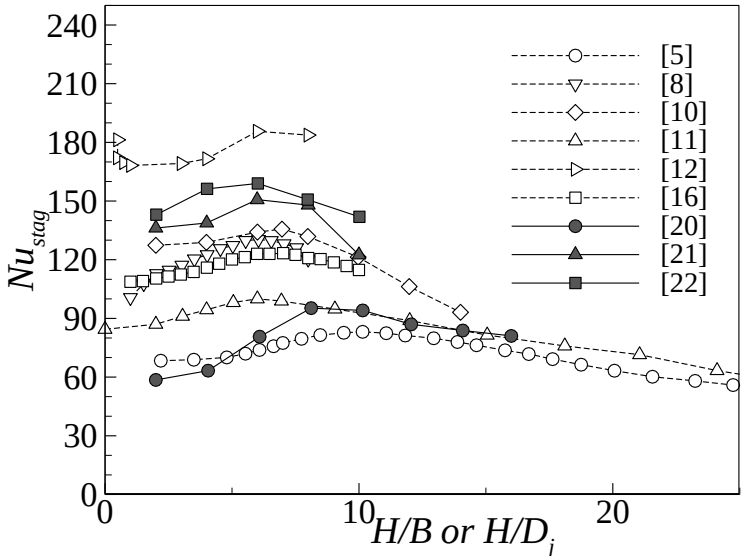

Figure 2. Heat transfer at the stagnation point, Nu_{stag} varied with a jet-to-target surface distance H normalized by a characteristic length, H/B or H/D_j where B is the slot width and D_j is the round jet diameter [5, 8, 10-12, 16, 20-22].

1.2. Objectives

The present study, therefore, aims to squarely address these ambiguities. To this end, a series of thermo-fluidic measurements has been conducted for a fixed jet Reynolds number based on the slot width and the jet centerline velocity of 20000, which ensures the fully turbulent jet whilst the jet exit-to-target surface distance varies from 3.0B to 16.0B under the constant heat flux input where B is the slot width.

2. EXPERIMENTAL DETAILS

2.1. Test Rig

Figure 3 shows a schematic of the present test rig consisting of a slot jet impinging on a target surface (a flat plate (0.5 m × 0.5 m) or a concave surface (D = 0.234 m)). Each target surface was fabricated from a 10 mm thick acrylic material (k ~ 0.2 W/mK). For heat transfer measurement, a film heating element (0.3 m × 0.3 m with thickness of 0.27 mm) was attached to the target surface, emitting a constant heat flux. Two foil and one bead-type pre-calibrated T-type thermocouples were used to measure the temperature at the stagnation point on the target surface, on the back of the target surface (to estimate heat loss), and at the slot exit, respectively.

Air at ambient conditions drawn by an axial fan controlled via an inverter was discharged from the slot with a fixed width of B = 0.026 m and height of L = 0.317 m. The target surface was mounted on a linear traverse system so that the slot exit-to-target surface distance, H/B, along the jet axis could be varied systematically.

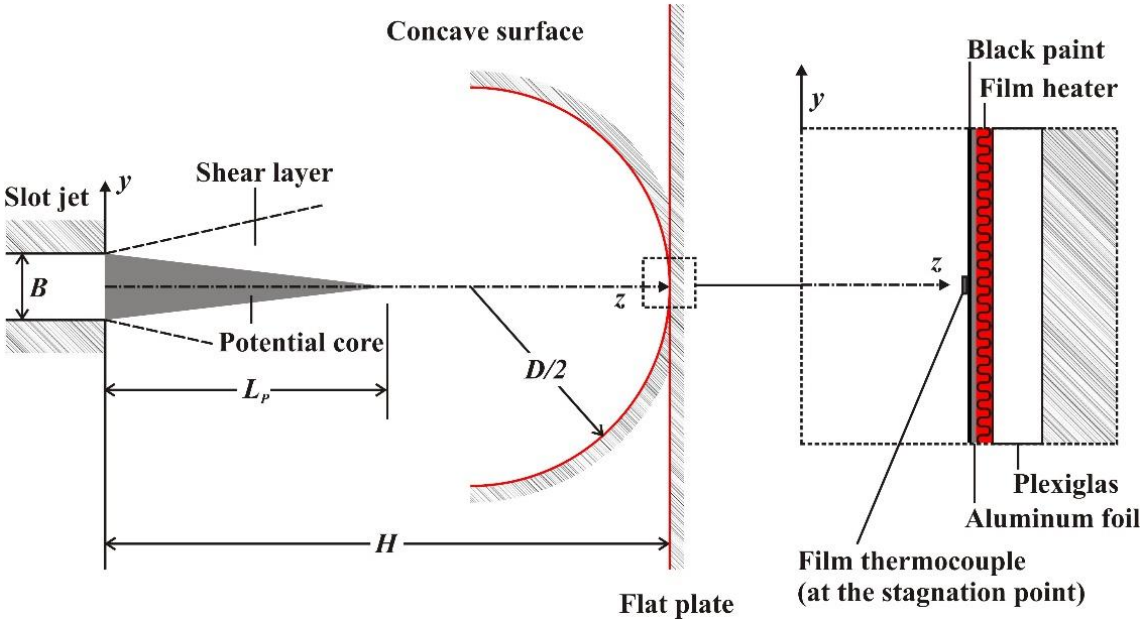

Figure 3. Schematic of the slot jet impingement on a flat plate or a concave surface (D/B = 9.0).

2.2. Pressure and Velocity Measurements

The velocity of the slot jet along the centerline axis (i.e., the z-axis) was measured to quantify the length of potential core with a Pitot tube in conjunction with a digital pocket

micro-manometer (DPM ST650^{TM}). The Pitot tube was linearly traversed along the centerline axis of the jet in free exit and in impingement on the target surface.

The jet Reynolds number based on the slot width (B) and jet centreline exit velocity (w_e) is defined as:

$$\mathrm{Re}_B = \frac{\rho w_e B}{\mu} \tag{1}$$

During the entire experiment, Re_B was fixed at 20000. The measurement uncertainty of the Reynolds number was estimated using a method reported in reference [27] (based on 20:1 odds) and found to be within 0.5%.

Static pressure distribution along the target surface was measured from pressure tappings drilled through the surface (the inner diameter of 0.6 mm) distributed laterally from the stagnation point and recorded by a differential pressure transducer (Digital Sensor Array (DSA^{TM}) Scanivalve Inc.). The local static pressure distribution was evaluated using the dimensionless pressure coefficient defined as:

$$C_p = \frac{p - p_e}{\rho w_e{}^2 / 2} \tag{2}$$

where p and p_e are the static pressures measured on the target surface at an arbitrary lateral location and at the jet exit, respectively. Each pressure value represents the average of 240 samples collected over a 10 second period. The measurement uncertainty of the pressure coefficient was estimated (based on 20:1 odds) and found to be within 1.7%.

2.3. Turbulence Measurement

To quantify the level of turbulence in the slot jet, the time-resolved velocity along the jet axis was measured using a single-sensor hot-wire probe (Dantec Dynamics MiniCTA^{TM}). The probe was linearly traversed along the jet axis in free exit and in impingement on a target surface. The root mean square velocity (w_{rms}) is defined as:

$$w_{rms} = \sqrt{\frac{1}{N}\sum_{1}^{N}(w_i')^2} \tag{3}$$

where w_i' denotes the measured instantaneous velocity fluctuation and N represents the number of samples. The turbulence strength has been obtained by normalising the root mean square velocity by the centre-line velocity at the jet exit (i.e., w_{rms}/w_e). The measurements were performed at a sampling frequency of 20 kHz over duration of 10 seconds, thus a total of 200000 samples. The experimental uncertainty of w_{rms}/w_e was estimated to be within 4.2%.

2.4. Flow Visualization Using Helium Bubbles

To visualize jet pattern confined between the jet exit and the flat plate (and the concave surface), a Helium bubble generator (Sage Action Inc. Model 5) was used. The neutrally buoyant bubbles used to seed the slot jet were generated by blowing a 1.5 mm Helium jet through a soap film in a moving air stream. The bubbles were transported using clean dry air to a cyclone centrifuge. The denser bubbles containing a mixture of air and Helium were removed from the bubbles leaving only the neutrally buoyant bubbles of 2 mm diameter. These bubbles were injected into the settling chamber to allow for the bubbles to accelerate before passing through the honeycomb flow straightener at the entrance to the slot jet.

The illumination for the flow visualization was provided by a Halogen light source. The light was focused to a fringe-less rectangular beam 25 mm wide along the *y*-axis in Fig. 3. The center of the beam was positioned at the mid-length plane of the slot jet along the *x*-axis.

The images were captured using a digital single-lens reflex (DSLR) camera mounted perpendicularly to the light beam a distance of 1 m above the beam. The camera was operated in manual mode with the ISO set at 100 for maximum resolution, the aperture was set at *f* 3.5 to allow for maximum light to enter the camera, a focal length of 18 mm was used to obtain a wide field of view and an exposure time of 6 seconds was used. This combination allowed for images of good resolution to be captured. The long exposure ensured that a single bubble could be followed. The images were processed (Gimp 2.8) using the histogram method of threshold manipulation. The low pixel intensity of any foreground or background items allowed these items to be eliminated from the image, leaving only the bubbles, the wall, and the slot jet exit visible.

2.5. Heat Transfer Measurement

The heat transfer characteristics were evaluated using the Nusselt number defined based on the slot width *B* as:

$$Nu_B = \frac{h_s}{k_f / B} \tag{4}$$

where

$$h_s = \frac{q''_{net}}{T_s - T_e} \tag{5}$$

Here, q''_{net} is the net heat flux, k_f is the thermal conductivity of air, whilst T_s and T_e are the local stagnation point surface temperature and jet temperature at the slot exit, z = 0, respectively. The net heat flux, q''_{net} is obtained through energy balance:

$$q''_{net} = q''_{t} - q''_{cond} - q''_{rad} \quad (6)$$

where q''_t is the total heat flux emitted from the film heating element, q''_{cond} and q''_{rad} are the conduction and the radiation heat loss, respectively. The conduction heat loss through the backside of the target surface was estimated using Fourier's law and found to be 3.5%. The radiation loss is calculated using Stefan–Boltzmann law:

$$q''_{rad} = \varepsilon\sigma(T_s^{\,4} - T_a^{\,4}) \quad (7)$$

Here, ε is the emissivity, σ is the Stefan–Boltzmann constant, and T_a is the ambient temperature. The emissivity was taken to be 0.94 as estimated by an infrared camera (FLIR^{TM} T-Series).

The resolution of the temperature readings from the temperature scanner was ±0.1 K for each thermocouple. The errors associated with the multimeter readings for the input voltage to/the electrical resistance of the film heater were estimated to be ±0.09 V and ±0.27 Ω, respectively, resulting in a total heat flux error of ±11.1 W/m^2. The uncertainty of the net heat flux was estimated to be within 1.1%. Therefore, the uncertainty of the Nusselt number was calculated to be within 3.3%.

2.6. Heat transfer mapping using an infrared (IR) thermography

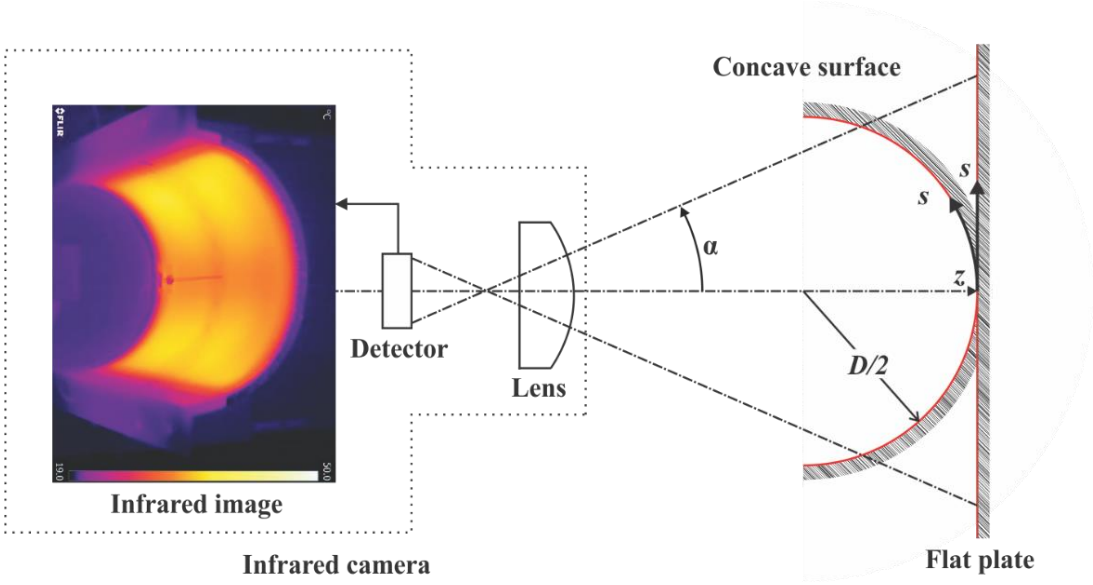

Figure 4. Schematic of infrared temperature measurement on a flat plate and concave surface.

Thermal radiation is the energy radiated by the surface of an object whose temperature is above absolute zero (0 K or -273.15°C). It propagates as an electromagnetic radiation, proportional to the object's temperature, and without the need of a medium. Part of this radiation is infrared radiation which can be captured and used to evaluate the temperature of the object.

Infrared (IR) thermography is a non-contact temperature measurement method which records infrared energy emitted from a body. It is typically used for steady or transient study of convective heat fluxes and complex fluid field, due to its high sensitivity (down to 20 mK), low response time (down to 20 µs), two dimensionality (from 80 k up to 1 M pixels, at 50 Hz) [28]. IR thermography works based on energy conservation, expressed as:

$$U_{tot} = E_{obj} + E_{refl} + E_{atm} \tag{8}$$

where U_{tot} is the total IR radiation captured, E_{obj}, E_{atm} and E_{refl} are the emission of the object, the emission of the atmosphere, and the reflection of the object and its surroundings respectively. After applying Stefan–Boltzmann's law and Planck's law, Equation (7) becomes:

$$U_{tot} = \varepsilon_{obj}\tau_{atm}\sigma({T_{obj}}^4) + (1-\varepsilon_{obj})\tau_{atm}\sigma({T_{refl}}^4) + (1-\tau_{atm})\sigma({T_{atm}}^4) \tag{8}$$

therefore

$$T_{obj} = \sqrt[4]{\frac{U_{tot} - (1-\varepsilon_{obj})\tau_{atm}\sigma({T_{refl}}^4) + (1-\tau_{atm})\sigma({T_{atm}}^4)}{\varepsilon_{obj}\tau_{atm}\sigma}} \tag{9}$$

where T_{obj}, T_{refl} and T_{amb} are the object, the reflected, and the ambient temperature respectively. ε_{obj} is the emissivity of the object, τ_{atm} is the transmittance of the atmosphere and σ is the Stephan-Boltzman's constant (5.6704 E-08 W/m^2 K^4). Typically, the transmittance of the atmosphere is estimated using the distance from the object and the relative humidity; the ambient temperature is measured with a thermometer; and the emissivity of the object and the reflected temperature are estimate in-situ [29].

Infrared thermography is generally achieved with the usage of an IR camera, equipped with a lens which role is to focus the IR energy onto a detector (either thermal detector, which is sensitive to the incident energy flux; or quantum, whose sensitivity depends on photon absorption) [28, 30], which generates an electrical signal proportional to the radiation; this signal is then amplified and transformed using successive digital signal processing into an image showing the temperature distribution as illustrated in Fig. 4.

Despite the benefits of IR thermography, it also has limitation in the form of many parameters which can cause an error of measurements; this includes parameters to consider during calibration (object emissivity, reflective temperature, ambient temperature, relative humidity, distance). For the current study, an infrared camera (forward-looking infrared (Flir) T-Series) was used to measure the local heat transfer distribution on a target surface, subjected to an impinging slot jet. The setting of the IR camera was configured as shown in Table 3. The emissivity was calibrated using the contact method described in Usamentiaga *et al*. [29] as follows:

- The target surface was heated without jet, until it reached temperatures similar to that during jet impingement.
- A film thermocouple flush mounted on target surface (at the stagnation point (Fig.4.)) was used to obtain a reference temperature.
- Once the target surface had reached temperatures similar to that during jet impingement, a reference temperature was measured with the thermocouple, then IR camera emissivity was changed until it detected a temperature matching with the reference temperature at the same location.

A second IR camera emissivity calibration method called reference emissivity material method is described in Usamentiaga *et al*. [29] and can also be used.

The reflected temperature was estimated using a method also described in Usamentiaga *et al*. [29] and ASTM E1862-97(2002)e1 [31]as follows:

- A crumpled and re-flattened piece of aluminium foil was used as a reflector.
- The re-flattened aluminium foil was positioned in the field-of-view of the IR camera.
- The temperature of the foil was measured with the emissivity and distance set at 1 and 0 on the camera.
- The reflected temperature was measured by applying the temperature of the foil to the surface the resulting temperature value is the reflected temperature.

Amongst other parameters causing a measurement error while using an IR camera, the view angle is commonly encountered, due the fact that it is not always possible to align the camera with the surface to be measured. To account the effect of the view angle, the temperature distribution on the target surface was captured with the IR camera for an isothermal case (without impinging jet). IR images were captured while constant uniform heat flux (10 W/m^2, 25 W/m^2, and 30 W/m^2) was maintained on the target surface. The IR images were processed using FLIR Tools+ software in order to extract the temperature

distribution along the *s*-axis, and compared to the thermocouple (at the stagnation point (Fig.4.)) measured temperature. The temperature of the thermocouple at 0° relative viewing angle was match to the thermocouple temperature at the same location by adjusting the emissivity setting on the IR camera.

Figure 5 (a) and 6 (a) shows that when the camera (lens) is positioned 1m away from both surfaces (flat plate and concave surface), the deviation of the temperature occurs at a relative viewing angle of approximately 4.45° and 3.55° for the flat plate and concave surface respectively, regardless of applied heat flux. This is due to the distortion of the image which begins to affect the infrared measured temperature at a smaller relative viewing angle on the concave surface compared to the flat plate. In reality, the actual viewing angle is higher on the concave surface compared to the flat plate at a same relative viewing angle due to the curvature of the concave surface. Additionally, it should be noted that the deviation of the temperature with the increase of relative viewing angle is more accentuated on the concave surface compared to the flat plate.

Perspective distortion defined as the warping of an object and its surrounding area due to its position relative to the camera, varies with the object-to-focal lens distances and the viewing angle at which the image is captured, causing the apparent relative distances to differ from the actual. In the current experiment the perspective distortion as a result of the relative viewing angle affect the uniformity of the pixel concentration (therefore the colour intensity) which is used to evaluate the temperature causing an error in measurement.

To correct errors associated with the view angle, the curves in Fig. 5 (b) and 6 (b) were used to derive a fourth order polynomial expression of the curve trend and shown in Table 3, which was used to correct error of IR temperature associated with the viewing angle.

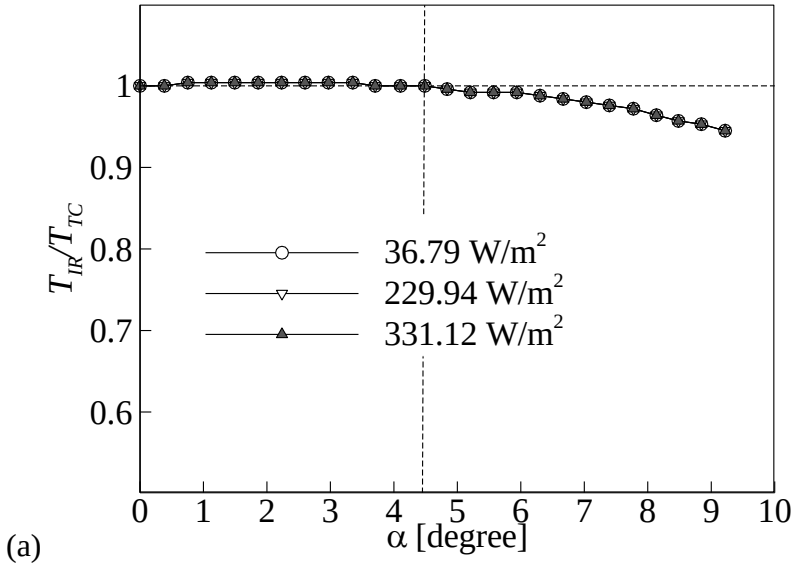

(a)

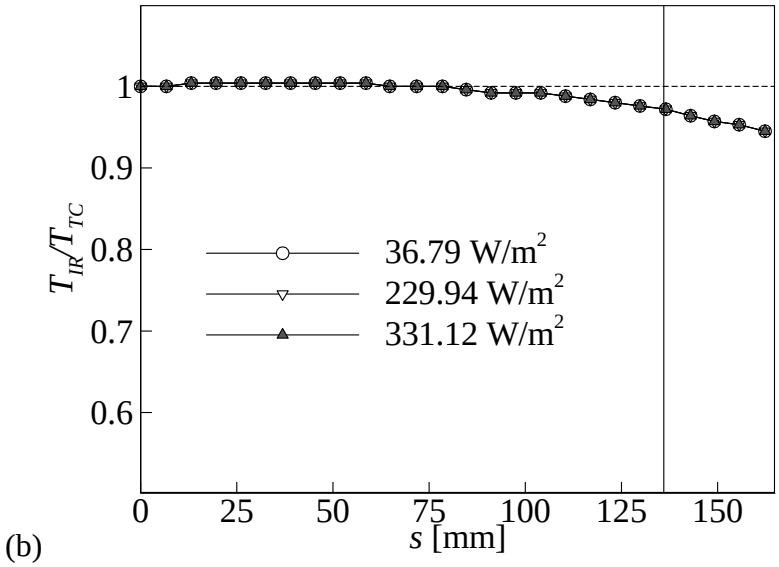

(b)

Figure. 5. Effect of viewing angle on IR temperature normalized by thermocouple temperature (T_{IR}/T_{TC}) on a flat plate versus (a) the IR camera relative view angle α, (b) the radial location *s*.

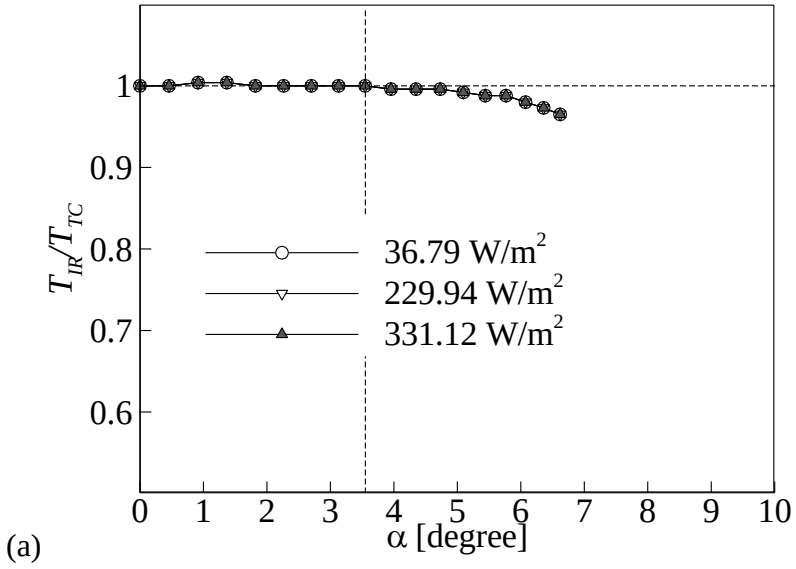

(a)

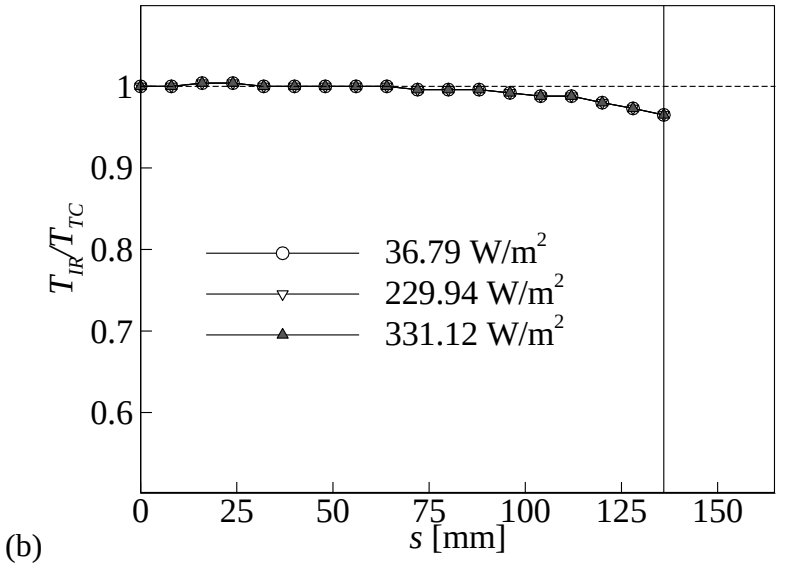

(b)

Figure. 6. View angle effect on IR temperature normalized by thermocouple temperature (T_{IR}/T_{TC}) on a flat plate versus (a) the IR camera relative view angle α, (b) the radial location *s*.

3. FREE SLOT JET CHARACTERISTICS

This study considers a two-dimensional un-confined jet (in the *y*-*z* plane at $x = 0$, Fig. 3) discharged to a surrounding fluid (of the same fluid properties) – submerged jet, removing heat from a target surface (both a flat plate and a concave surface). Therefore, it is instructive to establish the free slot jet characteristics.

According to the classical description of free jet structures [23, 24, 32], three distinctive flow regions exist: (a) the initial region, (b) the transitional region, and (c) the

fully developed region. In the initial region, the jet velocity along the jet centerline axis maintains its magnitude as high as that at the jet exit. In the transitional region the jet centerline velocity begins to decrease substantially, transitioning to the fully developed region where it decays. Furthermore, a region where the jet is undisturbed by the entrainment is present, the so-called "potential core." After the jet is fully developed, the axial velocity profiles become self-similar, collapsing onto a single curve that could be fitted using Gaussian distribution [23, 24].

Following the definition of Giralt *et al*. [33], the potential core length is the distance from the jet exit to a downstream location where the centerline velocity w_0 reaches 98 % of the jet exit velocity w_e. For slot jets, Martin [34] suggested that the core length persists up to $4B$. It is derived from Fig. 4(a) that the present free slot jet has the length of potential core, $z/B = 6.0$.

The level of turbulence of the free slot jet is also measured along the jet axis. Figure 4(b) shows the turbulence intensity (w_{rms}/w_0) which initially increases throughout the length of potential core. Outside the potential core, it substantially increases. The variation of turbulence strength (w_{rms}/w_e) which is a measure of the velocity fluctuation (w_{rms} defined in Eq. (3)) in an absolute manner i.e., being normalized by the jet exit velocity, w_e (as also plotted in Fig. 4(b). There exists a peak of turbulence strength roughly at z/B = 12.5. This peak has been conjectured to be responsible for the peak in local heat transfer at the stagnation point on a target surface although this turbulence strength is of the free slot jet.

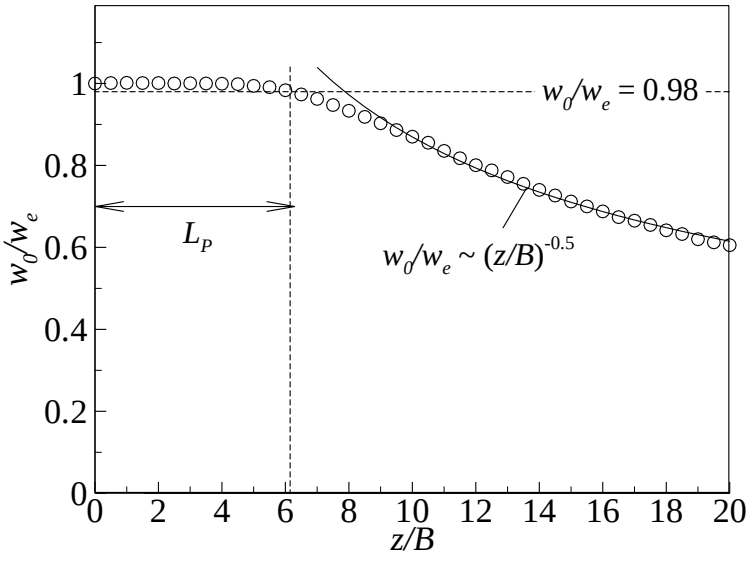

(a)

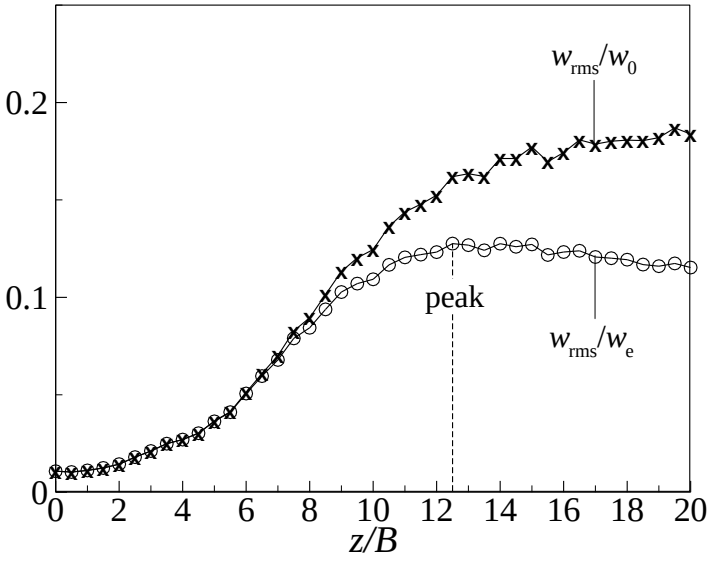

(b)

Figure 7. Variation of (a) Centerline velocity (w_0) and (b) Turbulence intensity (w_{rms}/w_0) and strength (w_{rms}/w_e), along the jet axis at Re_B = 20000.

4. Heat Transfer at the Stagnation Point on a Flat Plate

4.1. Heat Transfer at the Stagnation Point

Heat transfer at the stagnation point on a flat plate cooled by the fully turbulent impinging slot jet at Re_B = 20000 is characterized first as reference. Particular focus is placed on the clarification of the fluidic mechanism that determines a peak in heat transfer at the stagnation point, which occurs downstream of the tip of the potential core of the free jet. Figure 5 shows that as the flat plate is traversed away from the slot exit, heat transfer at the stagnation point is (a) slightly decreased, (b) reaching a local minimum at H/B = 5.5. After which, it is (c) increased gradually, (d) peaking at $9.5 \leq H/B \leq 11.0$, which is followed by (e) a monotonic decrease. The overall variation of heat transfer at the stagnation point with H/B is consistent with the previous studies data plotted in Fig. 2.

Considering the commonly adopted argument proposed by Gardon and Akfirat [5], there is a discrepancy. The peak in turbulence strength in Fig. 4(b) (for the present free slot jet) is located at z/B = 12.5 whereas heat transfer at the stagnation point peaks at $9.5 \leq H/B \leq 11.0$ in Fig. 5. Therefore, clarification is essentially required.

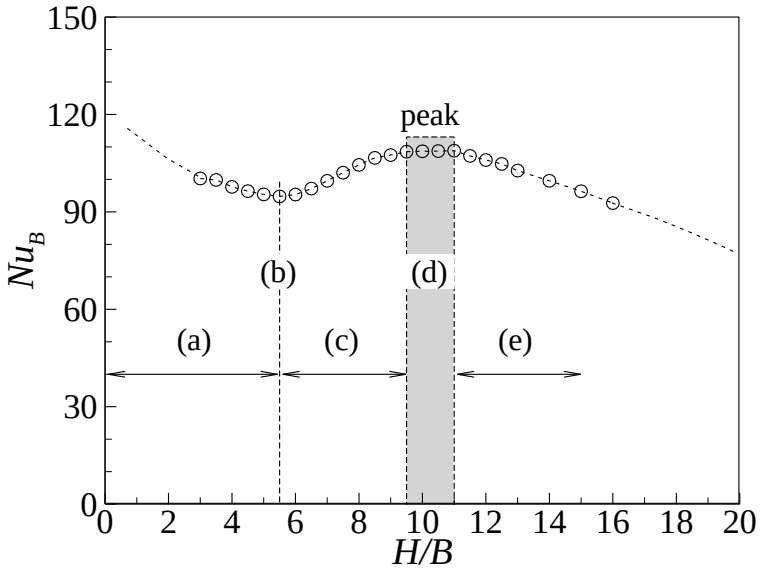

Figure 8. Heat transfer at the stagnation point Nu_B varying with the jet exit-to-flat plate distance H/B at Re_B = 20000.

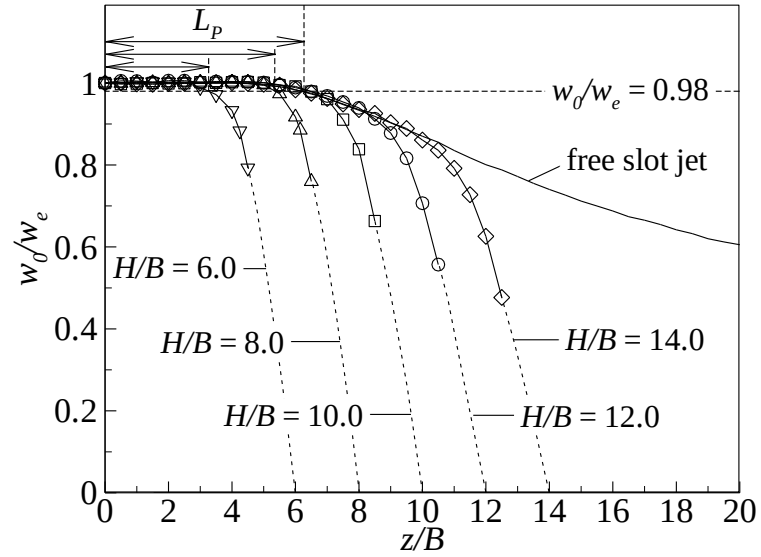

Figure 9. Variation of normalized centerline velocity along the jet axis with impingement on a flat plate at Re_B = 20000.

4.2. Centerline flow properties

The flow characteristics of the free slot jet in Fig. 4 are expected to vary due to the impingement on a flat plate. It has been argued [18, 23] that the jet region affected by the target surface is limited within $1.0B \sim 2.0B$ upstream from the surface and it is often termed "a deflection zone." The other flow regions remain unaffected.

Figure 9 shows the variation of the centerline velocity normalized by that measured at the jet exit, w_0/w_e with the jet impinging on the flat plate positioned at various H/B values.

Following the definition of Giralt *et al*. [33], the length of potential core of the present slot jet remains unchanged when $H/B > 10.0$ whereas the potential core is shortened when $H/B < 10.0$ (Fig. 6). It may be inferred from Fig. 6 that the deflection zone in the present configuration persists up to $3.0B$ upstream from the flat plate.

The discrepancy in the longitudinal peak locations between heat transfer at the stagnation point and turbulence strength may result from the changes in the jet flow characteristics during impingement. The centreline turbulence strength (w_{rms}/w_e) of the present slot jet along the jet centreline axis was measured during the impingement on the flat plate and results are plotted in Fig. 7(a). The flat plate is positioned at three selected axial locations, H/B = 8.0, 10.0, and 12.0.

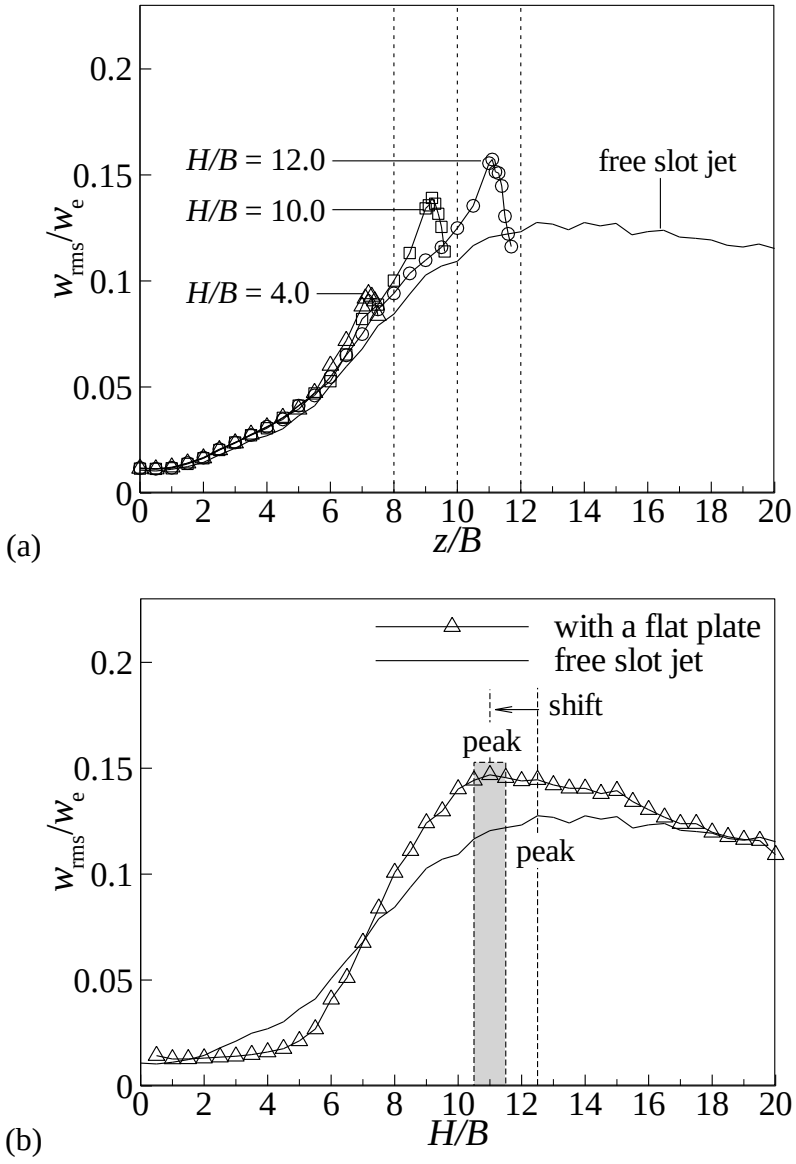

Figure 10. Turbulence strength (w_{rms}/w_e): (a) along the jet centerline axis (i.e., the z-axis); (b) at $0.5B$ upstream from a flat plate.

The turbulence strength with the flat plate initially follows the same trend as that of the free jet whose data are included in Fig. 7(a) as reference. It then peaks at roughly 1.0*B* upstream of the flat plate. In between the peak and the flat plate, there is a steep decrease in turbulence strength. It is evident that the variation of turbulent strength along the jet axis with the impingement on the flat plate substantially differs from that of the free slot jet.

To examine how the turbulence strength in the immediate proximity of the flat plate varies with *H/B*, the turbulence strength at 0.5*B* upstream of the flat plate was measured using a one-dimensional hot-wire probe fixed to the flat plate whilst varying *H/B* from 0.5 to 20.0. Results in Fig. 7(b) depict that with the flat plate positioned inside the potential core of the free slot jet, the turbulence strength is lower than that of the free jet. When the flat plate is positioned outside the potential core, it transitions to become higher than that of the free jet, eventually peaking in the range of $10.5 \leq H/B \leq 11.5$, which coincides with the longitudinal location of the peak in heat transfer observed in Fig. 5. In comparison, the turbulence strength data of the free slot jet, shows its peak at $H/B = 12.5$.

4.3. Summary

It can now be confirmed that the fluidic mechanism responsible for the peak in heat transfer at the stagnation point of the flat plate is the turbulence strength of the jet as previously conjectured. However, the longitudinal peak location of turbulence strength is shifted towards the jet exit by the flat plate, coinciding now exactly with the peak in heat transfer at the stagnation point.

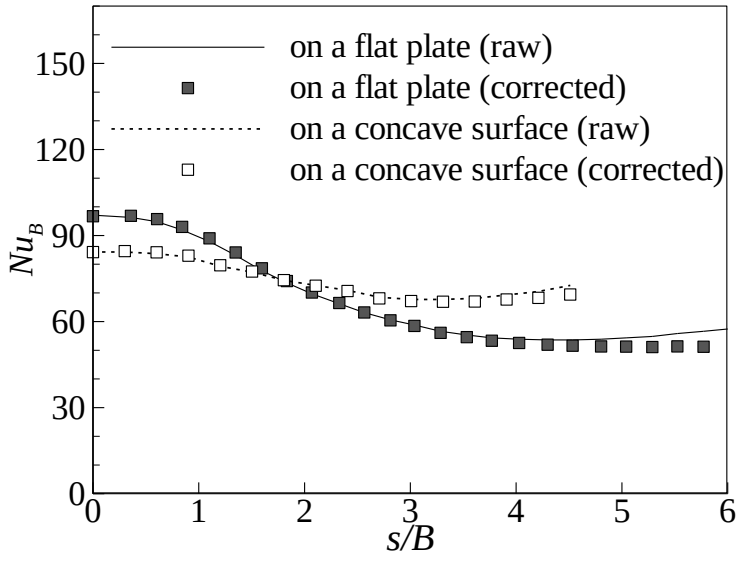

(a)

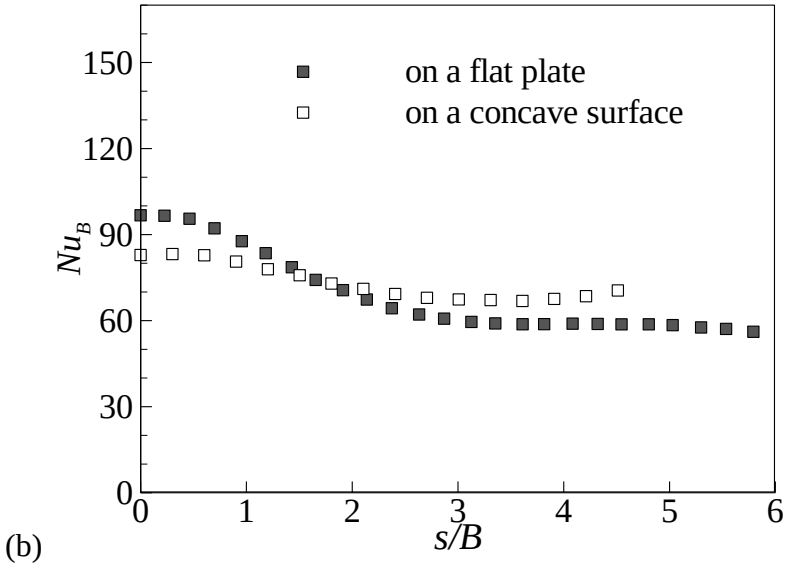

(b)

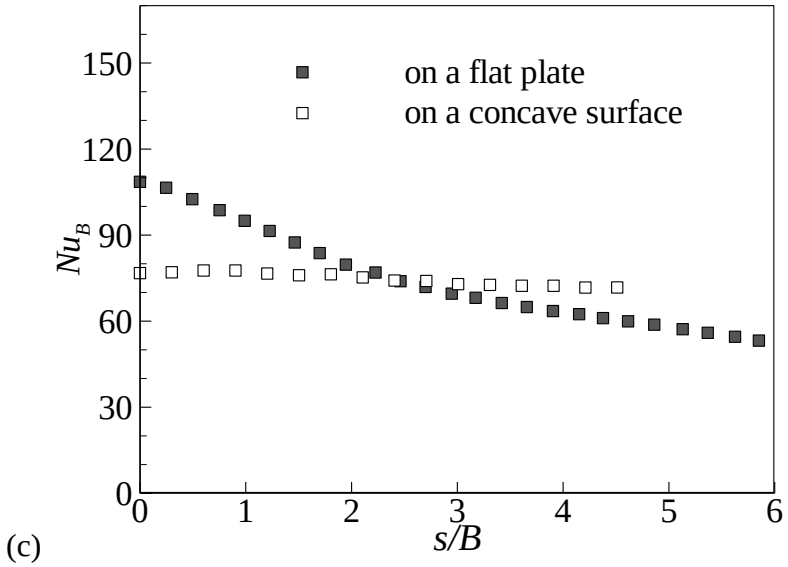

(c)

Figure 11. Local heat transfer along the flat plate and concave surface (D/B = 9.0), (a) H/B = 4.0, (b) H/B = 6.0, (c) H/B = 12.0.

5. HEAT TRANSFER AT THE STAGNATION POINT ON A CONCAVE SURFACE

The characteristics of slot jet impingement heat transfer on a flat plate serves as a reference configuration. It has been argued that higher average heat transfer can be achieved from a concave surface than from a flat plate, due to centrifugal instabilities on a concave surface resulting in the so-called “Görtler vortices” [18, 20, 22]. Figure 11 compares the local heat transfer distribution on the flat plate ($D/B = \infty$) with that on the small concave surface (D/B = 9.0) at three selected H/B values e.g., H/B = 4.0, 6.0 and 12.0, obtained using the pre-

calibrated infrared camera and corrected using fourth order polynomial in Table 2. In all cases, the highest heat transfer is located at the stagnation point and decreased along the s-axis (see, Fig. 11). At H/B = 4.0, which is inside the potential core of the present slot jet, there exists a second peak in heat transfer on the flat plate as a result of the transition from laminar to turbulent flow [5,8-12, 14-20]. For the same reason, there might be a second peak on the concave surface, which, however, cannot be fully observed due to the view angle distortion near the edge of the concave surface. At H/B = 12.0, the local heat transfer distribution on the concave surface is almost constant whereas that on the flat plate monotonically decreases from the stagnation point along the s-axis. It appears that the area-average heat transfer over the flat plate is lower than that over the concave surface, which is consistent with previous results [18, 20, 22]. However, it is interesting to notice that at the stagnation point, the flat plate provides higher local heat transfer than the concave surface regardless of the H/B values considered in the present study (Fig. 12), which is opposite to the area-average heat transfer.

5.1. Heat Transfer at the Stagnation Point

Heat transfer at the stagnation point of a concave surface (D/B = 9.0) that is subjected to the same slot jet impingement as the flat plate for Re_B = 20000 is characterized next. For a systematic comparison, the data for the flat plate under the identical conditions are included in Fig. 8. Heat transfer at the stagnation point (a) slightly decreases with H/B, (b) reaching a local minimum at H/B = 5.0. After which, (c) it gradually increases, (d) peaking approximately in the region of $7.0 \leq H/B \leq 9.5$, (e) followed by a sudden drop, and (f) a gradual decrease. The overall response is similar to that observed with the flat plate.

Distinctive differences from the flat plate are (i) the upstream shifting of the peak region from $9.5 \leq H/B \leq 11.0$ (on a flat plate) to $7.0 \leq H/B \leq 9.5$ (on a concave surface)), (ii) a sudden drop of Nu_B after the peak (at H/B = 9.5), and (iii) lower heat transfer (in magnitude) for the entire H/B range, which appears to be inconsistent with previous observations [18, 20]. In the following sections, these three differences are to be clarified.

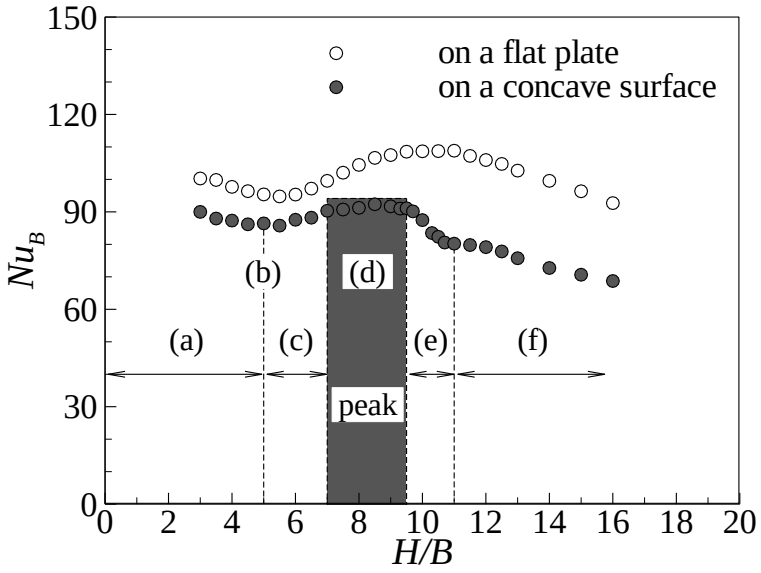

Figure 12. Heat transfer at the stagnation point of a concave surface cooled by a slot jet at Re_B = 20000 where the data for a flat plate under the same conditions are included for comparison.

5.2. Centerline Velocity

Figure 9 exhibits the shortening of the potential core regardless of the relative position of the concave surface. As the concave surface is positioned closer to the slot exit, the length of potential core is further shortened e.g., $L_p \sim 3.0$ for $H/B = 12.0$, $L_p \sim 2.5$ for $H/B = 10.0$, $L_p \sim 4.0$ for $H/B = 8.0$, and $L_p \sim 0.7$ for $H/B = 4.0$. There is a transition of L_p between $H/B = 10.0$ and 8.0, which requires elaboration to follow.

To identify a cause of the shortening of the potential core with the concave surface, a series of flow visualizations using Helium bubbles has been carried out. The flow image in Fig. 10(a) shows that the jet impinging on the flat plate is deflected laterally and leaving away from the stagnation point. However, with the concave surface, after stagnation the deflected jet follows the curvature of the concave surface and is re-circulated into the incoming jet (i.e., re-entrainment) as visualized in Figs. 10(b, c). The similar aerodynamic re-entrainment was also observed by Cornaco *et al.* [35].

The re-entrained flow then penetrates into the potential core, and eventually shortens its length. Based on these flow images, it may be inferred that if the slot is positioned within a certain distance e.g., $H/B < 9.5$, the re-entrained flow into the incoming jet is interfered by the slot. In this case, some portion of the re-circulated flow plays no part in the re-entrainment, forming "partial re-entrainment. However, if H/B is large enough e.g., $H/B > 9.5$, full re-entrainment takes place.

The significance of the partial and full re-entrainment is that the re-entrained flow acts to reduce the centreline velocity by diffusion whilst promoting flow mixing, leading to the reduction in heat transfer at the stagnation point. Furthermore, as observed in Fig. 8, there is a steep drop in heat transfer at the stagnation point after H/B = 9.5 with the concave surface, this can be referred to as the transition from partial to full re-entrainment.

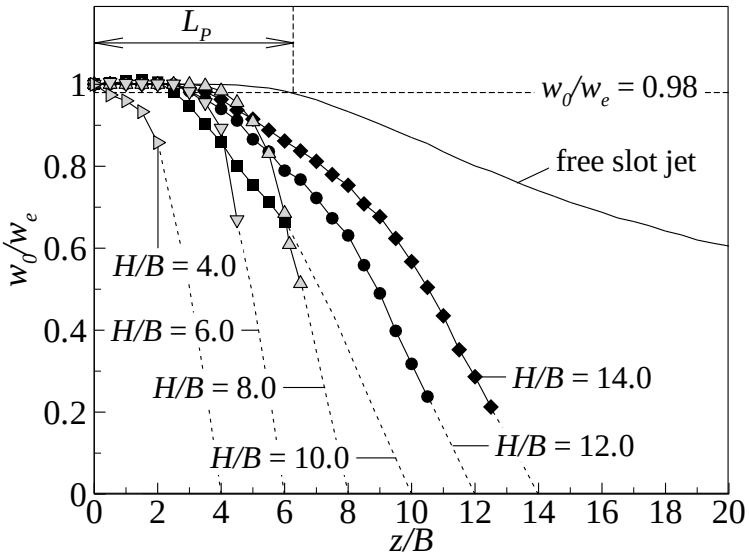

Figure 13 Variation of normalized centerline velocity along the jet axis (i.e., the *z*-axis) of a slot jet impinging on a concave surface at Re_B = 20000.

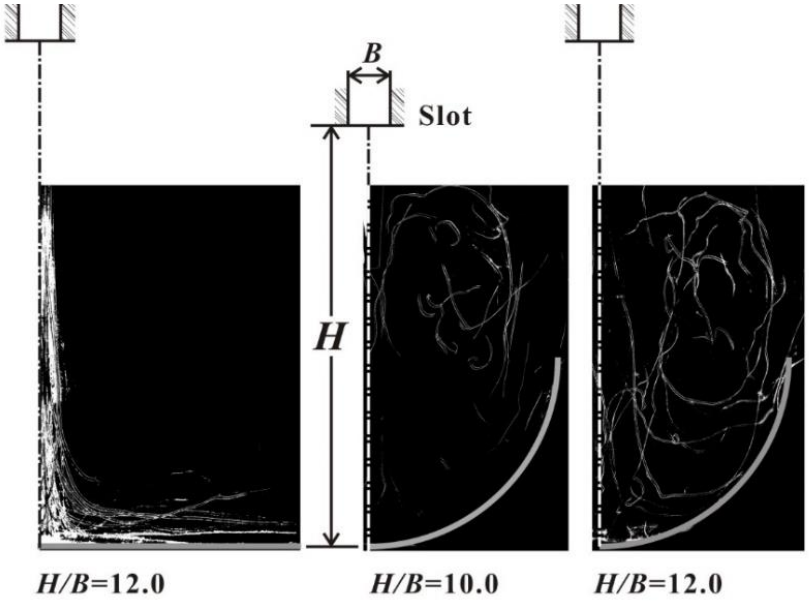

(a) (b) (c)

Figure 14. Streaklines of the slot jet impinging: (a) on a flat plate; (b and c) on a concave surface (D/B = 9.0), for Re_B = 20000.

5.3. Centerline Turbulence Strength

The aerodynamic re-entrainment is also expected to alter the level of turbulence along the jet axis. Figure 11(a) exhibits the variation of centreline turbulence strength (w_{rms}/w_e) of the present slot jet along the jet centerline axis with the concave surface. Similar to the case with the flat plate, the concave surface is positioned at three selected axial locations, H/B = 8.0, 10.0, and 12.0. The turbulence strength follows that of the free jet whose data is included in Fig. 11(a) as reference for a very short impinging distance after which it is suddenly increased. It is also noticeable that with the concave surface at H/B = 10.0 and 12.0, the turbulence strength steeply increased, deviating from that of the free jet. Moreover, the turbulence strength peaks at a shorter upstream location e.g., roughly at 1.5B upstream at H/B = 8.0, at 4.0B upstream at both H/B = 10.0 and 12.0. Similarly to the flat plate, in between the peak and the concave surface, there is a steep decrease of the turbulence strength.

The variation of turbulence strength measured at 0.5B upstream from the concave surface whilst varying H/B from 0.5 to 20.0 in Fig. 11(b) shows that the turbulence strength follows the same trend as that of the free jet until H/B = 3.5. After which, it increases steeply, peaking between $9.5 \leq H/B \leq 10.5$, followed by a sudden drop similar to heat transfer at the stagnation point observed in Fig. 8. It should be pointed out that this longitudinal location of the peak in turbulence strength overlaps with that in heat transfer at the stagnation point on the concave surface.

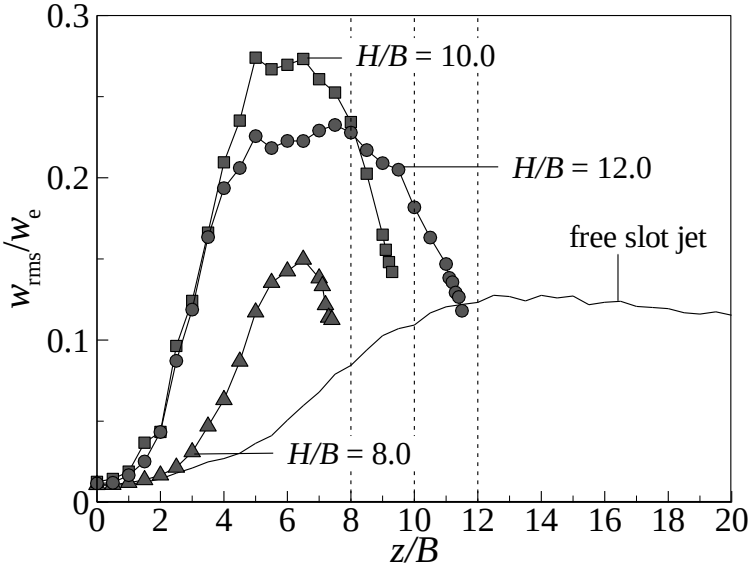

(a)

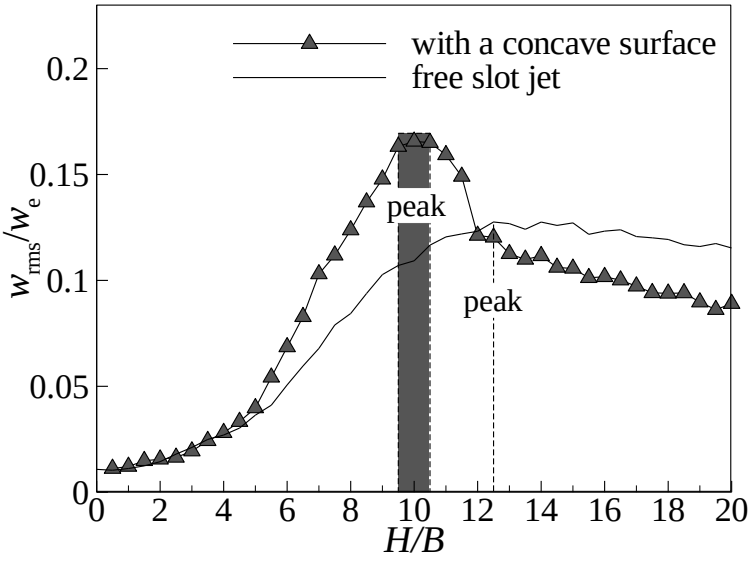

(b)

Figure 15. Turbulence strength (w_{rms}/w_e): (a) along the jet axis (i.e., the z-axis); (b) at 0.5B upstream of a concave surface.

5.4. Flow Acceleration near the Stagnation Point

Heat transfer at the stagnation point of both the flat plate and the concave surface and fluidic mechanisms responsible for the distinctive features have been discussed separately. Similar and dissimilar features of heat transfer at the stagnation point on both target surfaces that vary with the jet exit-to-flat plate (or concave surface) distance are compared in this section. Particular focus is placed on why heat transfer at the stagnation point on the concave surface (at least with D/B = 9.0) is lower than that on the flat plate in terms of magnitude.

It has been argued that heat transfer at the stagnation point is predominantly governed by flow acceleration [13, 14, 17]. According to the boundary layer theory [36-38], heat transfer at the stagnation point is directly proportional to the square root of the local velocity gradient (acceleration) at the stagnation point, as:

$$Nu_B \sim \left(\frac{dv_s}{ds}\right)^{0.5} \tag{9}$$

where v_s is the velocity component along the circumference (the s-axis).

Based on the measured pressure distribution near the stagnation point on both flat plate and concave surface and the Bernoulli's equation, the velocity component along the target surface has been calculated. Results are plotted in Fig. 13. The flow acceleration near the stagnation point is indicated by the slope of each curve. At both H/B = 4.0 and 12.0, the slopes of the flat plate are steeper than on the concave surface, leading to the observed higher heat transfer at the stagnation point on the flat plate.

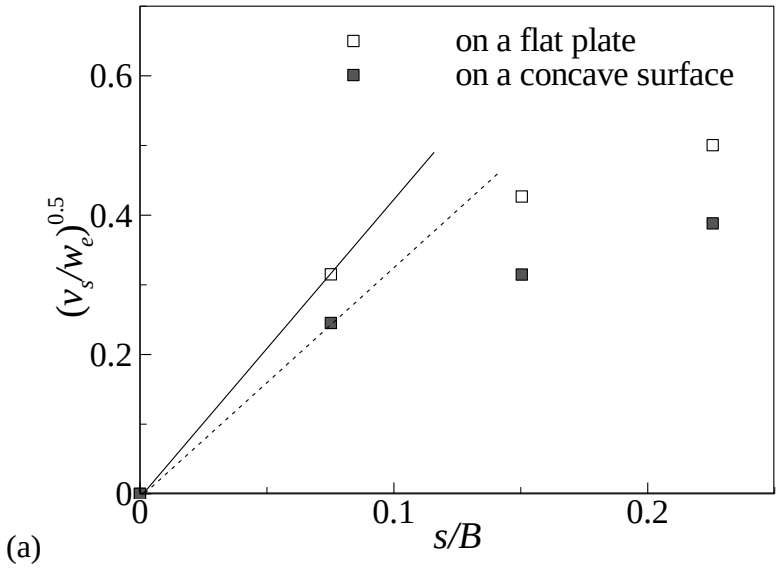

(a)

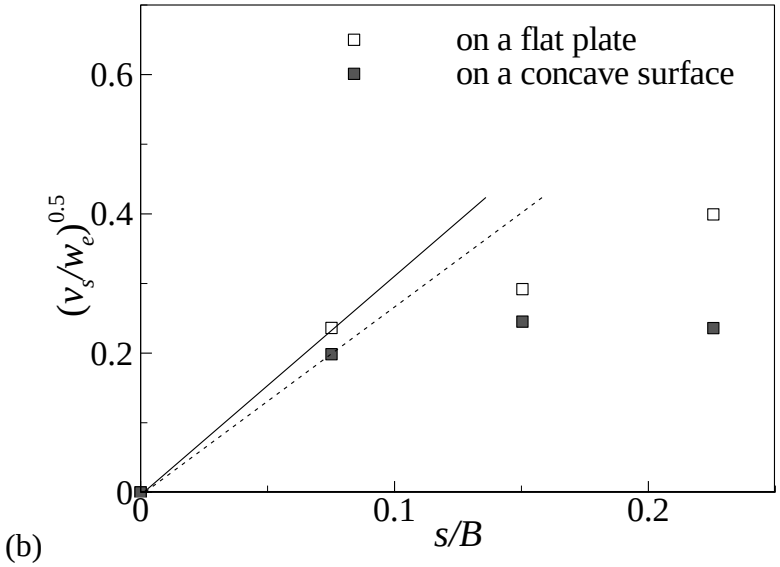

(b)

Figure 16. Flow acceleration: (a) lateral pressure distribution on the flat and concave surface; and lateral velocity normalized by the jet exit velocity v_s / w_e along the target surfaces, (b) at H/B = 4.0, (c) at H/B = 12.0.

6. SUMMARY

Heat transfer at the stagnation point of the concave surface varies with the jet exit-to-concave surface distance (H/B), similar to that with the flat plate. There is a peak region in heat transfer coinciding with the peak region in turbulence strength of the jet impinging on the concave surface which also varies with H/B. The jet length of potential core is shortened by the concave surface during the impingement. There is transition in heat transfer at the

stagnation point on the concave surface before and after $H/B \sim 9.5$ due to the transition from partial to full entrainment. If $H/B < D/B$, the partial re-entrainment takes place whereas if $H/B > D/B$, the full re-entrainment occurs further reducing heat transfer at the stagnation point on a concave surface.

Higher heat transfer at the stagnation point has been always obtained from the flat plate than from the concave surface for a given jet exit-to-target surface distance due to flow acceleration. However, it must be pointed out that the area-averaged heat transfer over a concave surface would be higher than that over the flat plate, consistent with previous results [18-20]. This is due to the fact that local heat transfer, highest at the stagnation point on the flat plate is laterally decreased faster from the stagnation point than that on the concave surface.

7. CONCLUSIONS

Fluidic mechanisms of heat transfer at the stagnation point of a concave surface as well as a flat plate cooled by a fully turbulent slot jet were identified. A series of experiments including flow visualisation, velocity profile, turbulence level, and pressure measurements was conducted at a fixed jet Reynolds number of 20000. New findings are summarized as follows.

(1) The previous conjecture on the fluidic mechanism of the non-monotonic variation of heat transfer at the stagnation point on a flat plate with a slot exit-to-target surface distance being turbulence strength along the centreline axis of the slot jet is confirmed to be valid.

(2) However, the noticed discrepancy of the longitudinal location between the heat transfer peak and the turbulence strength peak of the free jet is explained by the upstream shifting of the turbulence strength due to the target surface.

(3) The peak of heat transfer at the stagnation point on a concave surface takes place at a shorter slot exit-to-target surface distance (H/B) due to the aero-dynamic re-entrainment of the jet, which shortens the potential core.

(4) In comparison with the flat plate, the concave surface acts to promote lateral diffusion of the slot jet before impingement, resulting in less momentum and less flow acceleration from the stagnation point along the circumference for a given H/B, which provides lower heat transfer at the stagnation point than a flat plate.

8. REFERENCES

[1] Han, J. -C., Dutta, S., Ekkad, S.V., *Gas Turbine Heat Transfer and Cooling Technology*, Taylor & Francis, Boca Raton, 2000, pp. 18-20.

[2] de la Calzada, P., and Alvarez, J. J., "Experimental Investigation on the Heat Transfer of a Leading Edge Impingement Cooling System for Low Pressure Turbine Vanes," *ASME Journal of Heat Transfer*, Vol. 132, No. 12, 2010, pp. 122202-122210.

[3] Chupp, R. E., Helms, H. E., McFadden, P. W., "Evaluation of Internal Heat-Transfer Coefficients for Impingement-Cooled Turbine Air Foils," *AIAA Journal*, Vol. 6, No. 3, 1969, pp. 203-208.

[4] Tabakoff, W., and Clevenger, W., "Gas Turbine Blade Heat Transfer Augmentation by Impingement of Air Jets Having Various Configurations," *ASME Journal of Engineering for Gas Turbines and Power*, Vol. 94, No. 1, 1972, pp. 51-58.

[5] Gardon, R., and Akfirat, J. C., "The Role of Turbulence in Determining the Heat-Transfer Characteristics of Impinging Jets," *International Journal of Heat Mass and Transfer*, Vol. 8, No. 10, 1965, pp. 1261-1272.

[6] Hardisty, H., and Can., M., "An Experimental Investigation into the Effect of Changes in the Geometry of a Slot Nozzle on the Heat Transfer Characteristics of an Impinging Air Jet," *Proceedings of the Institution of Mechanical Engineers Part C Mechanical Engineering Science*, Vol. 197,No. 1, 1983, pp. 7-15.

[7] Goldstein, R. J., Behbahani, A. I., Kieger Heppelmann, K., "Streamwise Distribution of the Recovery Factor and the Local Heat Transfer Coefficient to an Impinging Circular Air Jet," *International Journal of Heat and Mass Transfer*, Vol. 29, No. 8, 1986, pp. 1227-1235.

[8] Ashforth-Frost, S., Jambunathan, K., Whitney, C.F., Ball, S. J., 1997, "Heat transfer from a Flat Plate to a Turbulent Axisymmetric Impinging Jet," *Proceedings of the Institution of Mechanical Engineers Part C Mechanical Engineering Science*, Vol. 211,No. 2, 1997 pp. 167-172.

[9] Ashforth-Frost, S., and Jambunathan, K., "Effect of Nozzle Geometry and Semi-Confinement on the Potential Core of a Turbulent Axisymmetric Free Jet," *International Communications in Heat and Mass Transfer*, Vol. 23, No. 2, 1996, pp. 155-162.

[10] Lee, D.H., Song, J., Jo, M.C., "The Effects of Nozzle Diameter on Impinging Jet Heat Transfer and Fluid Flow," *ASME Journal of Heat Transfer*, Vol. 126, No. 4, 2003, pp. 554-557.

[11] Zhou, D. W., and Lee, S. -J., "Forced Convective Heat Transfer with Impinging Rectangular Jets," *International Journal of Heat and Mass Transfer*, Vol. 50, No. 9-10, 2007, pp. 1916-1926.

[12] Katti, V., and Prabhu, S. V., "Experimental Study and Theoretical Analysis of Local Heat Transfer Distribution Between Smooth Flat Surface and Impinging Air Jet from a Circular Straight Pipe Nozzle," *International Journal of Heat and Mass Transfer*, Vol. 51, No.17-18, 2008, pp. 4480-4495.

[13] Nirmalkumar, M., Katti, V., Prabhu, S. V., "Local Heat Transfer Distribution on a Smooth Flat Plate Impinged by a Slot Jet," *International Journal of Heat Mass and Transfer*, Vol. 54, No. 1-3, 2011, pp. 727-738.

[14] Gulati, P., Katti, V., Prabhu, S.V., "Influence of the Shape of the Nozzle on Local Heat Transfer Distribution Between Smooth Flat Surface and Impinging Air Jet," *International Journal of Thermal Sciences*, Vol. 48, No. 3, 2009, pp. 602-617.

[15] Limaye, M.D., Vedula, R.P., Prabhu, S. V., "Local Heat Transfer Distribution on Flat Plate Impinged by a Compressible Round Jet," *International Journal of Thermal Sciences*, Vol. 49, No. 11, 2010, pp. 2157-2168.

[16] Wang, X. L., Motala, D., Lu, T. J., Song, S. J., Kim, T., "Heat Transfer of a Circular Impinging Jet on a Circular Cylinder in Crossflow," *International Journal of Thermal Sciences*, Vol. 78, 2014, pp. 1–8.

[17] Lytle, D., and Webb, B. W., "Air Jet Impingement Heat Transfer at Low Nozzle-Plate Spacings," *International Journal of Heat Mass and Transfer*, Vol. 37, No.12, 1994, pp. 1687–1697.

[18] Yang, G., Choi, M., Lee, J. S., "An experimental Study of Slot Jet Impingement Cooling on Concave Surface: Effects of Nozzle Configuration and Curvature," *International Journal of Heat Mass and Transfer*, Vol. 42, No. 12, 1999, pp. 2199-2209.

[19] Choi, M., Yoo, H. S., Yang, G., Lee, S. J., Sohn, D. K., "Measurements of Impinging Jet Flow and Heat Transfer on a Semi-Circular Concave Surface," *International Journal of Heat and Mass Transfer*, Vol. 43, No. 10, 2000, pp. 1811-1822.

[20] Gau, C. and Chung, C. M., "Surface Curvature Effect on Slot-Air Jet Impingement Cooling Flow and Heat Transfer Process," *ASME Journal Heat of Transfer*, Vol. 113, No. 4, 1991, pp. 858–864.

[21] Lee, D.H., Chung, Y. S., Won, S. Y., "Technical Note the Effect of Concave Surface Curvature on Heat Transfer from a Fully Developed Round Impinging Jet," *International Journal of Heat and Mass Transfer*, Vol. 42, No. 13, 1999, pp. 2489–2497.

[22] Lee, C. H., Lim, K. B., Lee, S. H., Yoon, Y. J., Sung, N. W., "A Study of Heat Transfer Characteristics of Turbulent Round Jet Impinging on an Inclined Concave Surface Using Liquid Crystal Transient Method," *Experimental Thermal and Fluid Science*, Vol. 31, No. 6, 2007, pp. 559–565.

[23] Gauntner, J. W., Hrycak, P., Livingood, J. N. B., "Survey of Literature on Flow Characteristic of a Single Turbulent Jet Impinging on a Flat Plate," NASA-TN-D-5652, 1970.

[24] Viskanta, R., "Heat Transfer to Impinging Isothermal Gas and Flame Jets," *Experimental Thermal and Fluid Science*, Vol. 6, No. 2, 1993, pp. 111-134.

[25] Jambunathan, K., Lai, E., Moss, M. A., Button, B. L., "A Review of Heat Transfer Data for Single Circular Jet Impingement," *International Journal of Heat and Fluid Flow*, Vol. 13, No. 2, 1992, pp. 106–115.

[26] Lee, D. H., Chung, Y. S., Kim, D. S., "Turbulent Flow and Heat Transfer Measurements on a Curved Surface with a Fully Developed Round Impinging Jet," *International Journal of Heat and Fluid Flow*, Vol. 18, No. 1, 1997, pp. 160–169.

[27] Holman, J. P., *Experimental Methods for Engineers*, McGraw-Hill, New York, NY, USA, 2012, pp. 63-79.

[28] Carlomagno, G. M., Cardone, G., "Infrared thermography for convective heat transfer measurements," *Experiments in Fluids*, Vol. 49, No 6, 2010, pp. 1187–1218.

[29] Usamentiaga, R., Venegas, P., Guerediaga, J., Vega, L., Molleda, J., Bulnes, F. G., "Infrared Thermography for Temperature Measurement and Non-Destructive Testing", Sensors (Basel), Vol. 14, No. 7, 2014, pp 12305-48.

[30] Optris GmbH "Basic principles of non-contact temperature measurement" URL: http://www.optris.com/downloads-infrared-cameras [cited 27 December 2015].

[31] ASTM E1862-97(2002)e1, "Standard Test Methods for Measuring and Compensating for Reflected Temperature Using Infrared Imaging Radiometers", ASTM International, West Conshohocken, PA, 1997, URL: http://www.astm.org.

[32] Abramovich, G. N., *The Theory of Turbulent Jets*, MIT Press, Cambridge, MA, USA, 1963, pp. 1-5.

[33] Giralt, F., Chia, C. -J., Trass, O., "Characterization of Impingement Region in an Axisymmetric Turbulent Jet," *Industrial and Engineering Chemistry Fundamentals*, Vol. 16**,** No. 1, 1977, pp. 21-28.

[34] Martin, H., "Heat and Mass Transfer Between Impinging Gas Jets and Solid Surfaces," *Advances Heat in Mass Transfer*, Vol. 13, 1977, pp. 1-60.

[35] Cornaro, C., Fleischer, A. S., Goldstein R. J., "Flow Visualization of a Round Jet Impinging on Cylindrical Surfaces," *Experimental Thermal and Fluid Science*, Vol. 20, No. 2, 1999, pp. 66-78.

[36] Schuh, H., and Persson, B., "Heat Transfer on Circular Cylinders Exposed to Free-Jet Flow," *International Journal of Heat Mass and Transfer*, Vol. 7, No. 11, 1964, pp. 1257-1271.

[37] Kumada, M., Mabuchi, I., Kawashima, Y., "Mass Transfer on a Cylinder in the Potential Core Region of a Two-Dimensional Jet," *Heat Transfer - Japanese Research*, Vol. 2, 1973, pp. 53-66.

[38] Miyazaki, H., Sparrow, E. M., "Potential Flow Solution for Crossflow Impingement of a Slot Jet on a Circular Cylinder," *ASME Journal of Fluids Engineering*, Vol. 98, No. 2, 1976, pp. 249-255.

Table 1. List of impingement cooling studies on a flat plate and concave surface where (a) jet exit-to-target surface distance (H/B or H/D_j); (b) length of potential core of the free jet (z/B or z/D_j); (c) location of peak in heat transfer at the stagnation point (H/B or H/D_j); (d) location of peak in turbulence strength (in free exit, z/B or z/D_j).

Reference	Test parameters	Comments on heat transfer at the stagnation point
Gardon and Akfirat [5] (1965)	Slot jet impingement on a flat plate at Re_B = 22000 with a slot width of B = 6.35 mm (a) H/B = 2.0 ~ 40.0; (b) z/B = 5.0; (c) H/B = 11.0; (d) z/B ~ 8.0	First to propose that jet turbulence strength (intensity) and centerline velocity are attributed to the non-monotonic variation of heat transfer at the stagnation point, based on free jet characteristics.
Ashforth-frost *et al.* [8] (1996)	Round jet impingement on a flat plate at Re_{Dj} = 20000 *w*ith a round jet diameter not presented (a) H/D_j = 1.0 ~ 8.0; (b) z/D_j = 5.0; (c) H/D_j = 6.0; (d) z/D_j = 6.0	Showed that the confinement of a round jet lowers local heat transfer especially at small nozzle-to-plate spacing. The peak of heat transfer at the stagnation point coincides with 1.0D_j downstream from the potential core tip. Regarding the mechanism, referred to [5].
Lee *et al.* [10] (2004)	Round jet impingement on a flat plate at Re_{Dj} = 23000 with a round jet diameter of D_j = 21.6 mm (a) H/D_j = 2.0 ~ 14.0; (b) z/D_j = 4.0; (c) H/D_j ~ 7.0; (d) z/D_j = 7.0 ~ 8.0	The effect of nozzle diameter on flow properties and heat transfer for a round jet impinging on a flat plate at fixed Reynolds numbers studied. The same observation and conclusion on the non-monotonic variation of heat transfer at the stagnation point as [5].
Zhou and Lee [11] (2007)	Slot jet impingement on a flat plate at Re_B = 18720 with a slot jet width of B = 11.08 mm (a) H/B = 1.0 ~ 30.0; (b) z/B = 4.0;	The thermo-fluidic properties of a slot jet impinging on a flat plate was considered and correlations of the local and average Nusselt numbers proposed. The same observation and

	(c) H/B = 6.0; (d) N/A	conclusion on the non-monotonic variation of heat transfer at the stagnation point as [5].
Katti and Prabhu [12] (2008)	Round jet impingement on a flat plate at Re_{Dj} = 23000 with a round jet diameter of D_j = 7.35 mm (a) H/D_j = 0.5 ~ 8.0; (b) N/A; (c) H/D_j = 6.0; (d) N/A	Higher heat transfer at the stagnation point is at smaller jet-to-nozzle distance. Farther downstream, the same observation and conclusion as [5].
Gulati *et al.* [14] (2009)	Square slot jet impingement on a flat plate at Re_B =15000 with a slot jet width of B = 17.0 mm (a) H/B = 0.5 ~ 12.0; (b) N/A; (c) H/B = 6.0; (d) N/A	For H/B < 1.0, high heat transfer is observed due to the acceleration of the jet through the gap between target plate and nozzle exit. Farther downstream, the same observation and conclusion as [5].
Wang *et al.* [16] (2014)	Round jet impingement on a flat plate at Re_{Dj} = 20000 with a round jet diameter of D_j = 30.0 mm (a) H/D_j = 1.0 ~ 10.0; (b) z/D_j = 4.0; (c) H/D_j = 6.0 ~ 7.5; (d) N/A	Local heat transfer on a cylinder impinged by a round jet, with particular focus on the effect cylinder-to-jet diameter ratio on local heat transfer studied. The same observation and conclusion on the non-monotonic variation of heat transfer at the stagnation point as [5].
Gau and Chung [20] (1991)	Slot jet impingement on a concave surface at Re_B = 20000 with a slot jet width of B = 20.0 mm (a) H/B = 2.0 ~ 16.0; (b) N/A; (c) H/B = 8.0; (d) N/A	The surface curvature effect on heat transfer on semi-concave and convex surfaces impinged by a slot jet, with focus on the local heat transfer distribution with an impinging distance. No comment on the non-monotonic variation of heat transfer at the stagnation point.

Yang *et al.* [18] (1999)	Slot jet impingement on concave surface and flat plate at Re_{2B} = 19200 (Re_B = 9600) with a slot jet width of B = 5.0 mm (a) H/B = 0.5 ~ 20.0; (b) z/B = 6.0; (c) H/B = 10.0; (d) z/B ~ 8.0	The effect of turbulent jet flow structure from different slot nozzle shapes on local and average heat transfer on a concave surface and a flat plate studied. The same observation and conclusion on the non-monotonic variation of heat transfer at the stagnation point as [5].
Lee *et al.* [21] (1999)	Round jet impingement on a concave at Re_{Dj} = 23000 with a round jet diameter of D_j = 34.0 mm (a) H/D_j = 2.0 ~ 10.0; (b) z/D_j = 4.0; (c) N/A; (d) z/D_j = 6.0~8.0	The local heat transfer and wall pressure coefficient for a round jet impinging on a concave surface reported. The same observation and conclusion on the non-monotonic variation of heat transfer at the stagnation point as [5].
Lee *et al.* [22] (2007)	Round jet impingement on a concave at Re_{Dj} = 23000 with a round jet diameter of D_j = 30.0 mm (a) H/D_j = 2.0 ~ 10.0; (b) N/A; (c) H/D_j = 6.0; (d) N/A	The effect on local and average heat transfer of inclining a concave surface cooled by round jet impingement studied. The same observation and conclusion on the non-monotonic variation of heat transfer at the stagnation point as [5]. Heat transfer at the stagnation point is increased with an increase in the surface curvature.

Table 2. Test parameters and conditions.

Test parameters	Value
Slot jet width, B	0.026 m
Slot jet height, L	0.317 m
Flat plate	0.5 m × 0.5 m
Concave surface diameter, D	0.234 m
Surface diameter-to-slot width ratio, D/B	Flat plate (∞), Concave surface (9.0)
Reynolds number, Re_B	20000
Total heat flux, q''_t	1174.5 W/m^2
Heating area	0.3 m × 0.3 m
Concave surface height	0.5 m

Table 3. Infrared camera settings.

Parameter	Value
Distance from the surface	1 m
Relative humidity	50%
Ambient temperature	20°C
Reflective temperature	20°
Surface emissivity	0.95 (calibrated in-situ with calibrated thermocouple)

Table 4. Infrared calibration fourth order polynomial.

Target surface	Polynomial
Flat plate	$T_{TC} = T_{IR}/ (-3E\text{-}10\ s^4 + 7E\text{-}08\ s^3 - 9E\text{-}06\ s^2 + 0.0004\ s + 0.9987)$
Concave surface	$T_{TC} = T_{IR}/ (-6E\text{-}10\ s^4 + 1E\text{-}07\ s^3 - 1E\text{-}05\ s^2 + 0.0003s + 0.9998)$